# New approach for the measurement of gas permeability and porosity accessible to gas in vacuum and under pressure

Hognon Sogbossi, Jérôme Verdier, Stéphane Multon

# New approach for the measurement of gas permeability and porosity accessible to gas in vacuum and under pressure

Hognon Sogbossi*, Jérôme Verdier, Stéphane Multon

*LMDC, Université de Toulouse, INSA, UPS, 135 Avenue de Rangueil, 31077 Toulouse cedex 04, France*

*Corresponding author: Email: sogbossi@insa-toulouse.fr

**Abstract:**

This study proposes new approaches for measuring the gas permeability and the accessible porosity of porous media. Two techniques are used: the usual permeameter, of the Cembureau type (measurement under pressure), and a new technique named a "double-cell" permeameter, based on a vacuum technique. Theoretical and experimental results point out that the apparent permeability measured in vacuum is proportional to the permeability measured under pressure. For a given pressure, the theoretical expression of the coefficients of proportionality leads to a quasi-constant value for a very large range of concrete permeability. A new equation is also proposed to evaluate the accessible porosity from the Time to Reach Steady State (TRSS) recorded during permeability tests. Concordance between the porosity accessible to gas obtained in this way and the porosity measured by the usual technique of hydrostatic weighing is discussed.

**Keywords:**

Transfer, permeability, porosity, vacuum, laminar flow, Knudsen flow.

# 1 Introduction

The viability of many structures depends on the concrete transport properties [1]–[5], which can be evaluated using the permeability. This permeability is quantified by the fluid flow through the porous medium under the effect of a pressure gradient. During permeability tests, the gas flow is quantified by measuring the volume flow rate through the porous medium in steady state (SS).

In the laboratory, flow measurements for gas permeability calculations are generally made under pressure with the Cembureau permeameter [6], [7]. This device needs a measurement cell and the specimen is inaccessible during flow measurements, so it is not easy to combine the gas permeability measurement with other tests [8]. Moreover, in situ permeability can be measured under vacuum. So, a new device that operates in low vacuum and is called a "double-cell" is used in this study. It can be used for example to perform monitoring of air permeability under a cyclic mechanical load [9].

The parameters that influence the gas flow rate and the corresponding permeability can be associated with the nature of the gas flow in the porous network [10]. In this paper, the term “flow regime” is used to name the nature of gas flows. The gas flow regime can be continuum or laminar flow, slip flow, transition flow, or free molecular or Knudsen flow [11]–[14]. Each flow regime contributes to the total apparent flow rate in a different proportion and the proportion can differ for measurements under pressure or in vacuum. For a better analysis of the permeability measurements, it is therefore important to first determine the contribution of each of the apparent flow modes to the total apparent flow [15]. In this study, the porous network is analysed using the time to reach steady state (TRSS), apparent permeability, and porosity. The TRSS is closely related to the characterization of connectivity and pore tortuosity [9], [16].

The transfer properties of concrete are strongly influenced by its connected porosity. The porosity of concrete is measured in the laboratory by hydrostatic weighing (the method described in standard NF P18-459 is generally used [6], [17]), by mercury intrusion, by nitrogen sorption or by water sorption [18]. These methods take quite a time to perform (generally one to two weeks) depending on the porosity range of the material. During the measurement of steady-state apparent flow, the TRSS is a function of the porosity, its connectivity and its fineness. Therefore, an original equation between the TRSS, the permeability (or flow rate) and the accessible porosity volume is proposed. In this paper, the porosity obtained with this method is compared to the accessible porosity to water obtained with usual hydrostatic weighing.

The first objective of this study is to establish and analyse an experimental database that compares permeability obtained from air flow measured in vacuum and under pressure. The second objective is the analysis of transfer properties to determine the characteristic permeability for an absolute test pressure of 2 bars, $k_{a2bars}$, and the intrinsic permeability $k_i$ using a single value of apparent permeability obtained in vacuum or under pressure. The third objective concerns a new approach for the calculation of porosity accessible to gas from the Time to Reach Steady State (TRSS).

# 2 Materials and methods

## 2.1 Materials

To compare the permeability obtained in vacuum and under pressure, tests were performed on two ordinary concretes [9], [19]. Their common characteristics are: the same cement CEM I 52.5 NCE CP2 NF: 320 kg/m$^3$ and the ratio Gravel / Sand is equal to 0.83. Plain concrete samples and reinforced samples were tested. Two batches of concrete (A and B) were used for the plain concrete samples. The ratios water / cement are respectively equal to 0.52 for batch A and 0.62 for batch B.

The concrete of batch A (W/C = 0.52) was used for some plain samples and was representative of the concrete walls of a power plant and was chosen as part of a national project [20]. The concrete of batch B (W/C = 0.62) was used for some plain samples and for reinforced samples.

Reinforced samples were used in order to test the limits of validity of the methods proposed in this paper. It was important to test the measurements and the analysis on samples with significant defects. Specific reinforced samples with embedded steel bars were used to obtain samples with preferential percolation paths as explained in [9], [19]. Such percolation paths have large impact on the apparent permeability of the sample and perhaps on their porosity. It was thus interesting to test the present method on such samples. Figure 1 presents all the configurations that were tested during this study and the water porosity of samples for drying at 105°C.

The length of the steel bars lay between 20 and 50 mm and the concrete sample thickness was 50 mm. A steel bar 50 mm long thus crossed the samples completely (Figure 1).

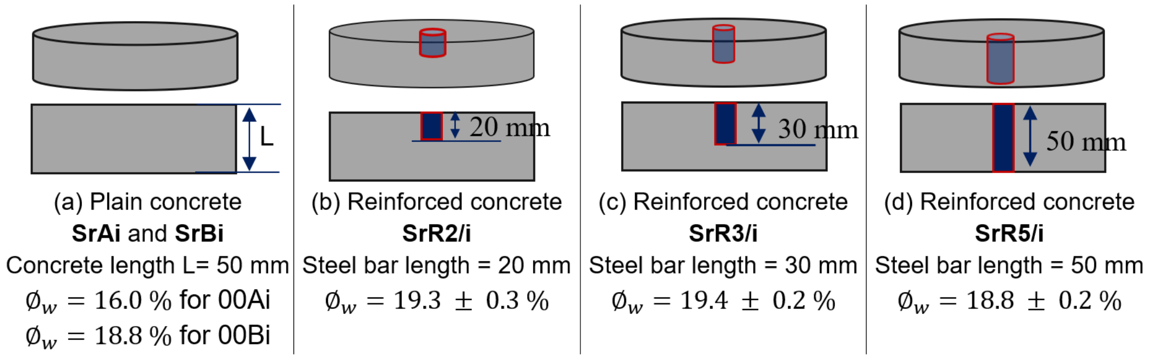


- Sr is the saturation degree; - i identifies the sample: i =1; 2; 3.

*Figure 1: Types and codes of samples [9], [19]*

## 2.2 Methods

### 2.2.1 Permeability

Flow measurements for gas permeability calculations are usually performed with the Cembureau permeameter in laboratory [6], [7]. The standard XP P 18-463 defines one permeability value as a standard: the apparent permeability calculated from the flow rate for an absolute test pressure of 2 bars. In this study this apparent permeability (designated as $k_{a2bars}$) is used as the characteristic permeability for a given sample.

Performing measurement of permeability under vacuum in laboratory [9] helps to better understand the permeability measurement devices which operate under vacuum used on site [21]. The gas flow regime differs according to the mechanism controlling the gas transfer (under pressure or in vacuum; in particular, the molecular free path is not the same under pressure and in low vacuum). This impacts the evaluation of the material permeability. The literature provides few information on permeability measurements in vacuum at steady-state or on the comparison between permeability measured under pressure and in vacuum. To obtain comparative results with the different methods used in the field and in laboratory, it is important, first, to acquire valid results for the two techniques on the same sample and then to analyse the determination of the permeability in the steady state with the vacuum technique. This is one of the objectives of the new “double-cell” device presented here.

### 2.2.2 Porosity

The accessible porosity is another fundamental property for transfer analysis. Until now, the methods used to evaluate this durability indicator have not always been relevant for the evaluation of the gas permeability of cementitious materials, as the porosity is often measured by a hydrostatic weighing method [6], [17]:

$$\emptyset_w = \frac{M_{air} - M_{dry}}{M_{air} - M_w} \times 100 \quad \text{(Eq. 1)}$$

where $\emptyset_w$ is the water porosity (%), $M_{air}$ is the mass of the saturated sample measured in air, $M_w$ is the mass of the saturated sample measured in water and $M_{dry}$ is the mass of the sample measured after drying.

The global theoretical porosity accessible to gas can be evaluated according to the saturation degree by:

$$\emptyset_{\mathrm{g}} = (1 - Sr)\emptyset_w \quad \text{(Eq. 2)}$$

where $\emptyset_{\mathrm{g}}$ is the porosity accessible to gas (%) and Sr the saturation degree.

Due to the geometry of the pores (connectivity, constrictivity, dead arms), water porosity cannot be exactly the same as the porosity accessible to gas that participates in the flow during a permeability test. Consequently, comparisons between experimental data on porosity-permeability and the predictive calculations performed with different models are often disappointing [22], [23]. Some researchers have explained these differences by the approximations made in the description of the microstructure in the models as well as on the uncertainties regarding the determination of their input quantities.

In addition, the measurement of porosity with a hydrostatic weighing method requiring drying in an oven may be potentially destructive for some specimens. Since the air does not react with the chemical components of cementitious material, a new approach for gas porosity calculation based on an air permeability test is proposed in this paper.

# 3 Experimental procedures

## 3.1 Permeability under pressure

Figure 2 gives an overview of the Cembureau apparatus [7], [24]. The main elements are: an air supply cylinder fitted with a pressure reducing valve, a precision pressure regulator, a pressure gauge, the permeability cell, a flow meter and a computer to record the air flow.

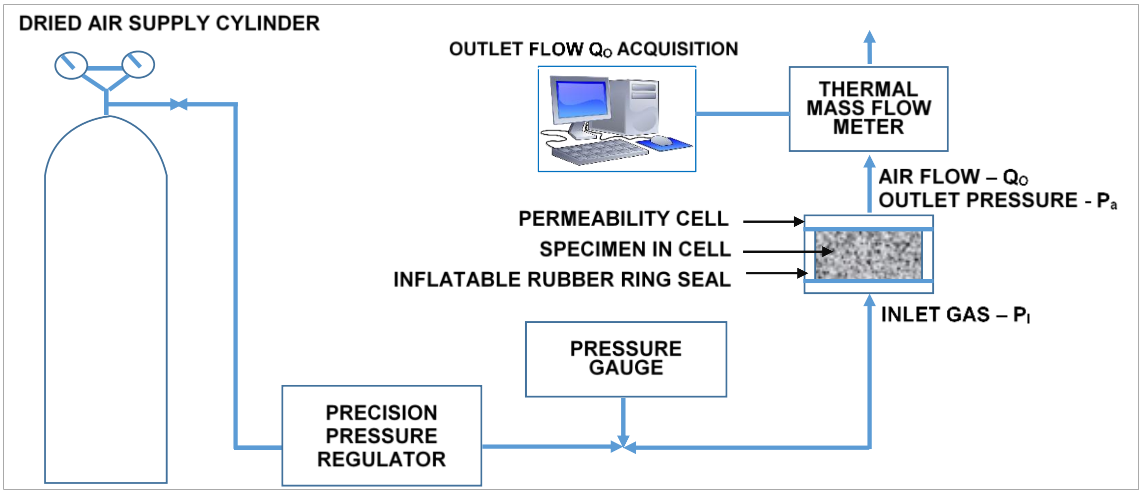


*Figure 2: Cembureau device for air flow measurement under pressure*

## 3.2 Permeability under vacuum

Figure 3 gives an overview of the double-cell apparatus to measure permeability under vacuum.

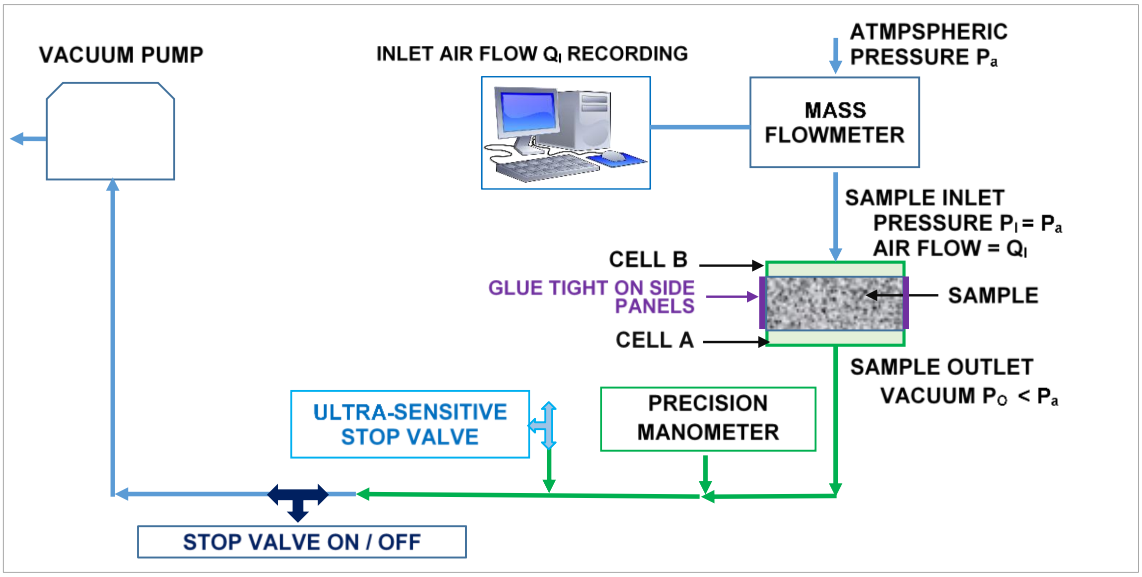


*Figure 3: Double cell device for air flow measurement under vacuum*

The air volume flow measurement protocol is the same as that of the Cembureau permeameter. However, the double cell device differs from the Cembureau by the following points:

- The permeability cell is replaced by two cells, one glued to each side face of the sample. The lateral faces of the sample are then sealed by means of a fixing / sealing glue. It is also possible to use the Cembureau cell when there is no necessity to access the sample during the test; this was done in the present study to perform under vacuum measurements in the same conditions as the measurements with the Cembureau technique on the same sample.

- The air supply bottle is replaced by a 4-head diaphragm vacuum pump (pump speed of 13 l/min), which facilitates the mobility of the double cell experimental device compared to the Cembureau device. The vacuum limit of the pump is 0.5 mbar.

The pressure regulator is replaced by an ultra-sensitive needle valve (Series 1300 straight-through, orifice 1.19 mm in 316 stainless steel). A manometer (Vacuubrand DCP 3000; pressure range 0.1 to 1080 mbar with digital display from 0.1 to 1100 mbar absolute) is used to measure the sample outlet pressure. Its accuracy is ± 1 mbar, which, according to our results, is sufficient since a variation of 1 mbar induces a maximum variation of 0.1% on the apparent permeability.

The reproducibility of test has been studied [9]. In all cases (plain concrete samples or reinforced concrete samples), the maximum relative errors obtained are lower than 1.5% for the air flow Q, 1.5% for the apparent permeability, and 3% for the TRSS.

### 3.3 Conditioning of samples

To obtain different values of porosity accessible to gas, the samples were tested at different saturation degrees. To achieve each saturation degree, the samples underwent precise conditioning [9]. This conditioning was inspired by the literature [25]–[27] trying to reduce the water gradient and associated cracking during conditioning.

The specimens were weighed before and after the permeability measurements. No mass variations were noted whatever the saturation degree, meaning that the global degree of saturation stayed constant during the test.

# 4 Theoretical approach

## 4.1 Permeability

### 4.1.1 Principle

The coefficient of permeability is defined by Darcy's law. The gas apparent permeability of a porous medium is calculated using the Hagen-Poiseuille relationship for laminar flow of a compressible fluid through a porous medium under steady-state conditions [24].

$$k_a = \frac{2\,\mu\,L}{S({P_I}^2 - {P_O}^2)} PQ \qquad \text{(Eq. 3)}$$

where $PQ$ is the inlet or outlet gaseous flow ($P_I Q_I$ or $P_O Q_O$), $P_I$ and $P_O$ are respectively the inlet and the outlet pressures (N.m$^{-2}$), $Q_I$ and $Q_O$ are respectively the inlet and the outlet volume flow rate (m$^3$.s$^{-1}$), $S$ is the cross-sectional area of the specimen (m$^2$), $L$ is the thickness of the sample in the direction of flow (m), and $\mu$ is the dynamic viscosity of the fluid (N.s.m$^{-2}$).

The principle of measuring permeability in the steady state is thus based on the measurement of the air flow $Q$ crossing a sample subjected to a pressure gradient. The difference between the two techniques used in this paper lies in the range of pressure applied to create the gradient and the position where the air flow is measured:

- Cembureau technique (under pressure): *the absolute applied pressure is the inlet pressure ($P_I$),* which is greater than atmospheric pressure ($P_a$), and the outlet pressure ($P_O$) is the atmospheric pressure, $P_a$. The air flow measured is the outlet one and, in Figure 2, $PQ = P_a Q_O$.
- Double-cell technique (in vacuum): the absolute inlet pressure ($P_I$) is equal to atmospheric pressure, *the absolute applied pressure is the outlet pressure ($P_O$),* which is less than atmospheric pressure (vacuum). The air flow measured is the inlet one and, in Figure 3, $PQ = P_a Q_I$ [9].

Klinkenberg linear theory (Eq. 4) is then used to determine the intrinsic permeability from the mean pressure. Klinkenberg established that a linear relationship can be assumed between the measured gas permeability ($k_a$) and the inverse of the mean pressure ($1/P_m$):

$$k_a = F_{Kl} k_i = k_i \left(1 + \frac{b_k}{P_m}\right) = \underbrace{k_i}_{Laminar} + \underbrace{k_i b_k / P_m}_{non-laminar} \qquad \text{(Eq. 4)}$$

where $k_a$ is the apparent permeability (also designated $k_{aP}$ in this paper to mention the pressure, P, applied during the test), $k_i$ is the intrinsic permeability, $F_{Kl} = 1 + b_K/P_m$ is the

Klinkenberg correction factor, $P_m$ is the mean pressure, and $b_K$ is the Klinkenberg gas slippage factor defined by [28]:

$$b_k = \frac{4c\lambda P_m}{r} = \frac{0.268}{r} \qquad \text{(Eq. 5)}$$

where $c \approx 1$ [13] and $\lambda P_m = 0.067$ µm.bar for air at a given pressure and r is the characteristic radius in µm.

### 4.1.2 Mean pressure during measurement

The evolution of the apparent permeability with pressure is thus generally plotted as a function of the inverse of the mean pressure. As a linear profile of pressure is often assumed in steady state, the mean pressure is evaluated by $(P_I + P_O)/2$. But, the pressure profile P(x) in concrete in the steady state is not linear because of the gas compressibility [16], [29], [30] and the mean pressure $P_m$ should not be taken equal to $(P_I + P_O)/2$.

In the steady state, the pressure profile P(x) can be evaluated from the following differential equation [16], [31]:

$$\left(\frac{dP}{dx}\right)^2 + P\frac{d^2P}{dx^2} = 0 \qquad \text{(Eq. 6)}$$

One solution of this equation has been derived by Verdier [19] as presented below:

$$P(x) = \left(\frac{{P_O}^2 - {P_I}^2}{L}x + {P_I}^2\right)^{1/2} \qquad \text{(Eq. 7)}$$

where $P_I$ is the sample inlet pressure and $P_O$ its outlet pressure.

By using the theorem of the mean value, we can deduce the true mean pressure in the steady state as follows [9]:

$$P_m = \frac{1}{L}\int_0^L \left(\frac{{P_O}^2 - {P_I}^2}{L}x + {P_I}^2\right)^{1/2} dx \qquad \text{(Eq. 8)}$$

The mean pressure $P_m$ can thus be evaluated from:

$$P_m = \frac{2}{3}\left(\frac{{P_O}^3 - {P_I}^3}{{P_O}^2 - {P_I}^2}\right) \qquad \text{(Eq. 9)}$$

This value is used in the following analysis.

### 4.1.3 Flow regime during measurement

To evaluate permeability reliably with Klinkenberg theory, the flow regime existing during the measurement must be known. The Knudsen number is a dimensionless parameter commonly used to classify flow regimes in small pores, where deviation from continuum flow is important. This is the case for cement-based materials. It is defined as the ratio of the molecular mean free path, λ (μm), to a characteristic length, such as pore radius, r (μm), and is given by:

$$Kn = \frac{\lambda}{r} = \frac{1}{r}\left(\frac{0.067}{P_m}\right) \quad \text{(Eq. 10)}$$

Where $P_m$ is the mean pressure in bar and the mean free path is evaluated by $\lambda P_m = 0.067$ μm.bar for air at a given pressure [28]. The determination of the radius r, characteristic of the percolation in a porous medium such as concrete is often difficult and constitutes a challenge [14]. Theoretical and empirical equations can be proposed to approximate this characteristic mean radius from a single apparent permeability [9]. The Knudsen number could then be calculated based on this equivalent radius and thus on the type of flow regime identified.

Flow regimes can be classified according to the Knudsen number as shown in Figure 4.

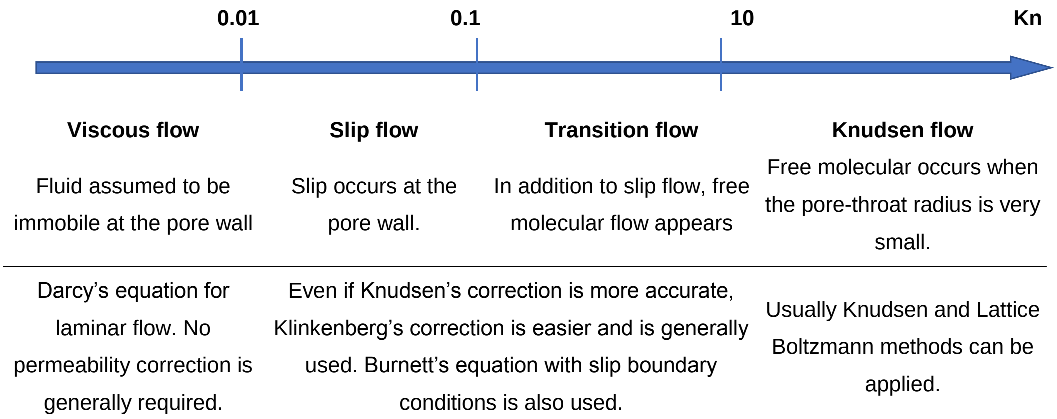


*Figure 4: Knudsen number, flow regime classifications for porous media [14], [32], [33]*

The flow regime in a cementitious porous material is generally a transition flow between laminar, slip and molecular regimes [14]. So, in this study, from Figure 4, we firstly make the assumption that the Knudsen number lies between 0.1 and 10. This allows us to use the Klinkenberg theory for the determination of the intrinsic permeability as is usually done in the literature.

The range of characteristic radius, r, that satisfies this condition can be theoretically deduced from the Knudsen number range (Eq. 10). By combining the two ranges of pore radius calculated (considering the lowest mean pressure used in this paper is 0.67 bar for the measurement in vacuum and 1.5 bars for the measurement under pressure), it is theoretically assumed here that Klinkenberg’s correction can be applied for r lying between 0.01 and 0.4 µm. These assumptions on Knudsen number and on the pore radius, r, have been verified from the permeability calculations. Kn is always found to be lower than 10 under pressure and in a vacuum. The flow regime is then a transition between laminar and molecular flow. It indicates that the application of Klinkenberg's theory is possible [9].

#### 4.1.4 Comparison of permeability obtained under pressure and under vacuum

Relations between Klinkenberg equations (Eq. 4) and (Eq. 5) can be used to establish a relation between the reference permeability, $k_{a2bars}$, obtained under pressure and the apparent permeability obtained in a vacuum, $k_{a\boldsymbol{P}}$. As $4c\lambda P_m = 0.268\ \mu m.bar$ for any air pressure [34], the Klinkenberg equation can be rewritten as:

$$k_a = k_i\left(1 + b_k \frac{1}{P_m}\right) = k_i\left(1 + \frac{4c\lambda P_m}{r}\frac{1}{P_m}\right) = k_i\left(1 + \frac{0.268}{r}\frac{1}{P_m}\right) \qquad \text{(Eq. 11)}$$

So, the ratio between the apparent permeability for $P_I$ = 2 bars and the apparent permeability for a given $P_I$ = P is:

$$\frac{k_{a\mathbf{2bars}}}{k_{a\boldsymbol{P}}} = \frac{k_i\left(1 + \frac{0.268}{r}\frac{\mathbf{1}}{\mathbf{1.568}}\right)}{k_i\left(1 + \frac{0.268}{r}\frac{\mathbf{1}}{\boldsymbol{P_m}}\right)} = C_{\boldsymbol{P}} \qquad \text{(Eq. 12)}$$

This ratio between apparent permeability is then:

$$k_{a2bars} = C_{\boldsymbol{P}}\, k_{aP} \qquad \text{(Eq. 13)}$$

where $C_P$ is a theoretical, non-dimensional coefficient:

$$C_P = \frac{r + 0.171}{r + 0.268/P_m} \qquad \text{(Eq. 14)}$$

where $r$ is the characteristic radius and $P_m$ is the mean pressure in bar.

Figure 5 presents the evolution of $C_P$ with the characteristic radius, r.

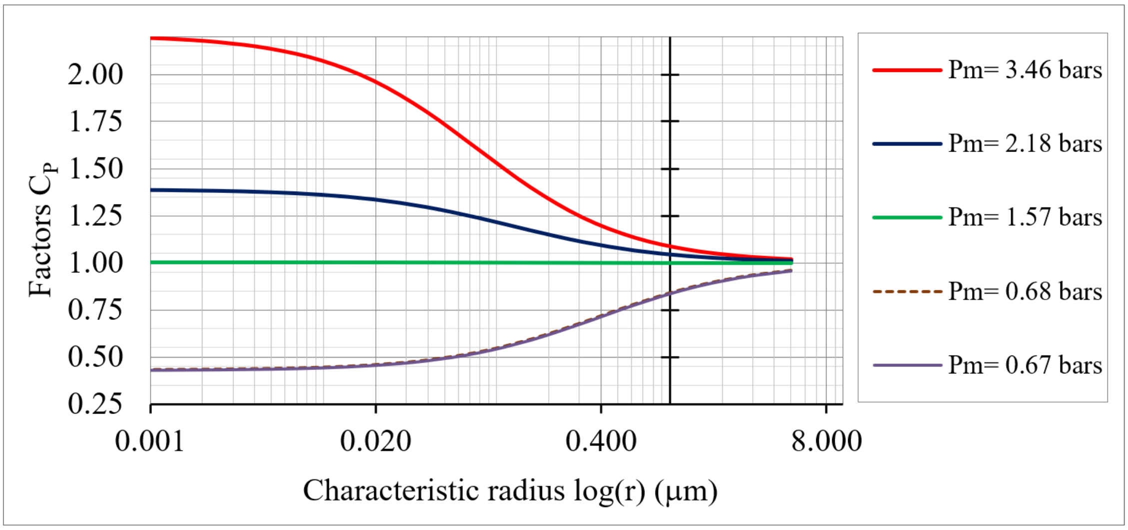


*Figure 5: Evolution of $C_P$ as function of characteristic radius r*

When r is very small, $C_P$ is high for under pressure measurement: the slip flow evaluated through the Klinkenberg slippage factor, $b_K$, is high. This is in accordance with the evolution of the Knudsen number: Kn is inversely proportional to radius r (Eq. 10), so Kn is higher for smaller r. When r increases, the Knudsen number decreases, the slippage factor $b_K$ also decreases, and the flow regime tends to laminar flow. For very large radius, the apparent permeability is equal to the intrinsic permeability. This occurs with highly porous media, such as rubberized cement-based composite [35].

In the range assumed in this paper for the pore radius r, in cementitious materials (r lies between 0.01 and 0.4 µm - this assumption has been verified in [9]) the coefficient $C_P$ shows small variations (Figure 5). A mean value of $C_P$ can be used, evaluated with the mean value theorem as:

$$\text{Mean value of } C_P = \frac{1}{0.4 - 0.01} \int_{0.01}^{0.4} \left( \frac{r + 0.171}{r + 0.268/P_m} \right) dr \qquad \text{(Eq. 15)}$$

The mean values of $C_P$ are presented in Table 1. Without knowing the real value of r, the relation of (Eq. 13) can be used to evaluate the apparent permeability as a function of the mean pressure given in Table 1.

**Table 1.** Main values of $C_P$ when r is between 0.01 and 0.4 µm as a function of the mean pressure $P_m$

| Measurement technique | Absolute Pressure (bars) | | | | $C_P$ (Eq. 15) |
|---|---|---|---|---|---|
| | Inlet $P_I$ | Outlet $P_O$ | Mean $P_m$ $(P_I + P_O)/2$ | Mean $P_m$ (Eq. 9) | |
| Cembureau | 2.0 | 1.013 (1 atm) | 1.51 | 1.57 | 1.00 |
| | 3.0 | | 2.01 | 2.18 | 1.17 |
| | 4.0 | | 2.51 | 2.81 | 1.30 |
| | 5.0 | | 3.01 | 3.46 | 1.41 |
| Double cell | 1.013 (1 atm) | 0.0005 | 0.51 | 0.67 | 0.61 |
| | | 0.050 | 0.53 | 0.68 | 0.61 |
| | | 0.150 | 0.58 | 0.69 | 0.62 |
| | | 0.250 | 0.63 | 0.71 | 0.63 |

4.1.5 Permeability determination

We can thus propose the calculation of intrinsic permeability from a single reference value $k_{a2bars}$. Using (Eq. 13) and $C_P$ values in Table 1, $k_{a2bars}$ can be calculated from any apparent permeability obtained under vacuum with the double cell technique. With (Eq. 13) and $C_P$ values in Table 1, the apparent permeabilities $k_{a3bars}$, $k_{a4bars}$, $k_{a5bars}$ can be calculated from a single $k_{a2bars}$. The intrinsic permeability $k_i$ can then be extrapolated to infinite pressure by plotting $k_{a2bars}$, $k_{a3bars}$, $k_{a4bars}$, $k_{a5bars}$ as a function of the inverse of the mean pressure (Klinkenberg theory). In the following, the calculated coefficients $C_P$ are validated on the experimental database established in this paper and then on some literature data.

## 4.2 Measurement of porosity accessible to gas

Porosity accessible to gas can be calculated from the TRSS and apparent permeability. This equation is based on the balance of the number of air particles flowing in the porous network due to the application of the pressure gradient to the steady state. For the sake of simplicity, only the demonstration based on measurement with the double-cell technique under vacuum is presented. The same demonstration can be made under pressure and gives the same results as the solution does not imply any particular assumptions.

The initial conditions for the test with the double-cell technique are first recalled:

- The flow is unidirectional along the length, L, of the sample.

- The pressure profile in the concrete is P(x). The boundary conditions are those described in Figure 3: the inlet pressure, $P_I$, is equal to the atmospheric pressure, $P_a$, at x = 0 and the outlet pressure is $P_O$ at x = L.
- t is the time during which the vacuum is applied; its maximum value is the TRSS (noted $t_{RSS}$ in the following equations). It is the time beyond which the mass flow is constant in any cross section of the sample. It is also the time beyond which the pressure profile in the concrete no longer varies.
- Y is the thickness of the sample reached by the vacuum pressure at any time t.

Figure 6 shows the evolution of pressure profile in concrete during air flow measurement.

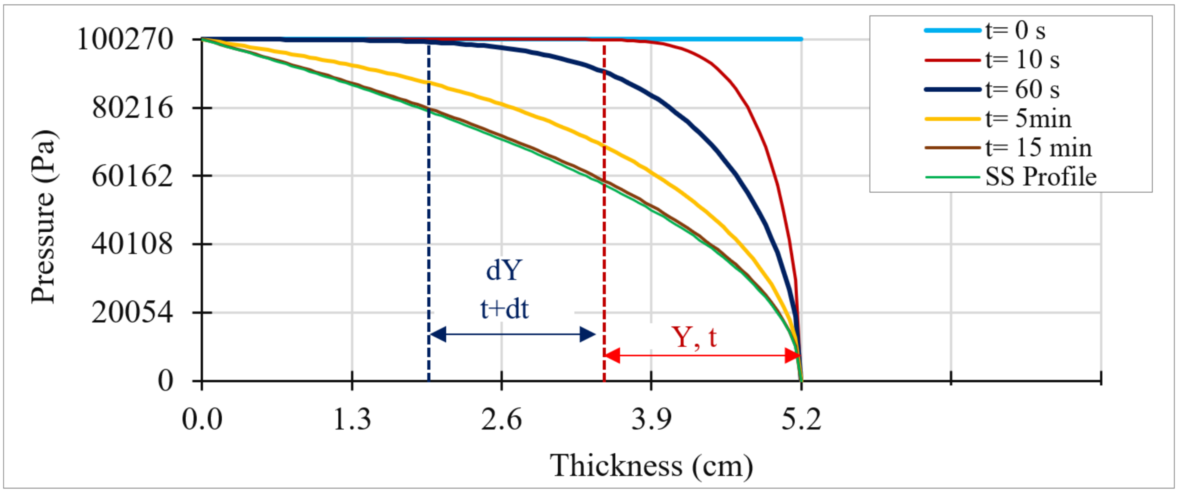


*Figure 6: Evolution of pressure profiles until steady state for a sample (L = 5.2 cm) [9]*

At the beginning of vacuum application, t = 0 s and the depth impacted by the vacuum is $Y_0$ = 0. At any moment t (t > 0) at the beginning of the application of the vacuum (10 s for example), a depth Y is impacted by the vacuum.

The air volume of the pores impacted during this time t and the corresponding number of air particles are, respectively:

$$V = AY\emptyset_g \quad \text{(Eq. 16)}$$

$$N = \frac{P_m.V}{B.T} = \frac{P_m}{BT}SY\emptyset_g \quad \text{(Eq. 17)}$$

where $P_m$ is the mean pressure at depth Y impacted by the vacuum during t (s), V is the air volume in pores of the zone impacted by the vacuum ($m^3$), S is the area of the sample section, $\emptyset g$ is the porosity accessible to gas and B is the Boltzmann number.

During any time interval dt, the vacuum affects a new front of air particles dN since the depth Y increases by dY. From (Eq. 17), it can be written:

$$dN = \frac{S\,\emptyset_{\mathrm{g}}}{BT}\,P_m dY \qquad \text{(Eq. 18)}$$

Also, the Hagen-Poiseuille equation (Eq. 3) gives the volume, dV, of gas flowing in the cell under the pressure gradient $(P_1 - P_2)$ over the distance Y into concrete.

$$dV = \frac{k_{ad}S}{2\mu}\,\frac{{P_I}^2 - {P_O}^2}{P_O Y}\,dt \qquad \text{(Eq. 19)}$$

This volume of air is at the outlet pressure $P_O$ and, in terms of the number of air particles, it corresponds to:

$$dN = \frac{P_O dV}{BT} \qquad \text{(Eq. 20)}$$

From the three previous relationships, it can be written:

$$dN = \frac{P_O dV}{BT} = \frac{P_O}{BT}\frac{k_{ad}}{2\mu}\,\frac{{P_I}^2 - {P_O}^2}{P_O Y}\,Sdt = \frac{S\,\emptyset_{\mathrm{g}}}{BT}\,P_m dY \qquad \text{(Eq. 21)}$$

After simplification, it can be deduced that:

$$YdY = \frac{k_a\left({P_I}^2 - {P_O}^2\right)}{2\mu\emptyset_{\mathrm{g}}P_m}\,dt \qquad \text{(Eq. 22)}$$

In the steady state, the mean pressure $P_m$ has reached its stabilized value so, by integrating the previous relation, the depth affected by the vacuum at any time t can be calculated from:

$$\frac{1}{2}Y^2 = \frac{k_a\left({P_I}^2 - {P_O}^2\right)}{2\mu\emptyset_{\mathrm{g}}P_m}\,t \qquad \text{(Eq. 23)}$$

At the steady state, $t = t_{RSS}$, Y = L, and $P_m$ is given by (Eq. 9), so the porosity can be evaluated from:

$$\emptyset_{\mathrm{g}} = \frac{k_a\left({P_I}^2 - {P_O}^2\right)}{\mu L^2 P_m}\,t_{RSS} = \frac{3}{2}\frac{k_a}{\mu L^2}\,\frac{\left({P_I}^2 - {P_O}^2\right)^2}{{P_I}^3 - {P_O}^3}\,t_{RSS} \qquad \text{(Eq. 24)}$$

Considering the Hagen-Poiseuille equation (Eq. 3), $\emptyset_{\mathrm{g}}$, the porosity accessible to gas, can also be written as a function of the measured air flow $PQ_V$:

$$\emptyset_{\mathrm{g}} = \frac{1}{SL}\left(\frac{2PQ}{P_m}\,t_{RSS}\right) = \frac{3PQ}{SL}\left(\frac{{P_O}^2 - {P_I}^2}{{P_O}^3 - {P_I}^3}\right)t_{RSS} \qquad \text{(Eq. 25)}$$

where the gaseous flow $PQ_V$ is the same as used in (Eq. 3). It is equal to $P_aQ_O$ if the Cembureau technique is used and $P_aQ_I$ with the double-cell technique. Regarding the sample,

$SL$ is the total apparent volume and the expression $2PQt_{RSS}/P_m$ can leads then to an estimation of the volume of percolating pores.

# 5 Results and discussion

## 5.1 Permeability under vacuum and under pressure

### 5.1.1 Experimental results

Figure 7 presents the apparent permeability, $k_a$, as a function of the inverse of the mean pressure $P_m$ for one sample of each type: one plain sample from batch A (a), one plain sample from batch B (b), one each of reinforced samples R2, R3 and R5 (c). The results obtained on the other samples led to the same analysis.

The apparent permeability under vacuum ($1/P_m > 1$) is always greater than the permeability under pressure obtained under pressure with the Cembureau permeameter ($1/P_m < 1$). This result is consistent with the evolution of the molecular and slip flows as the non-laminar contribution to air flow is inversely proportional to the pressure (Eq. 4). As the mean pressure with the double-cell under vacuum is always lower than the mean pressure in conditions of under pressure (Table 1), the apparent permeability under vacuum conditions must be greater than the one obtained under pressure.

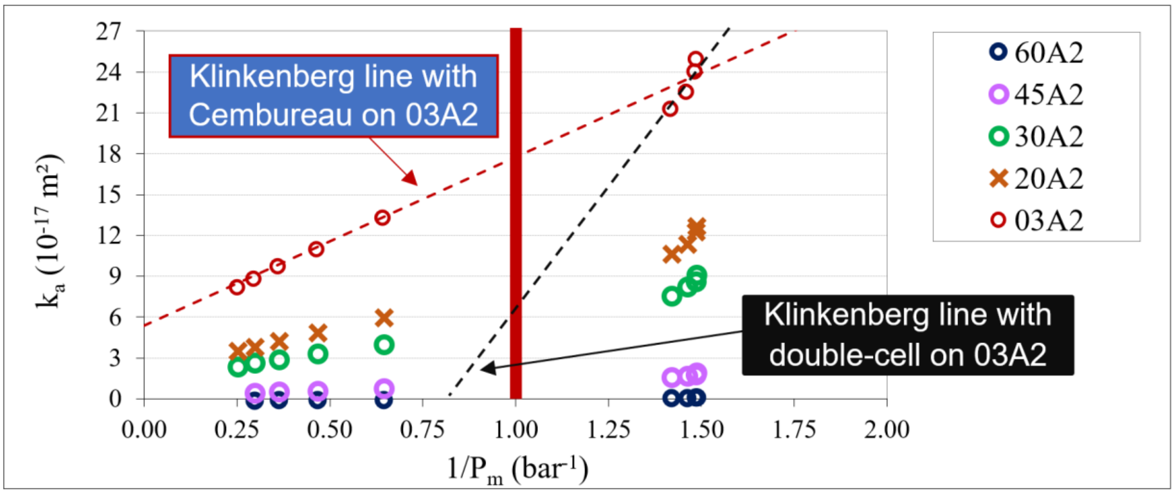


(a)

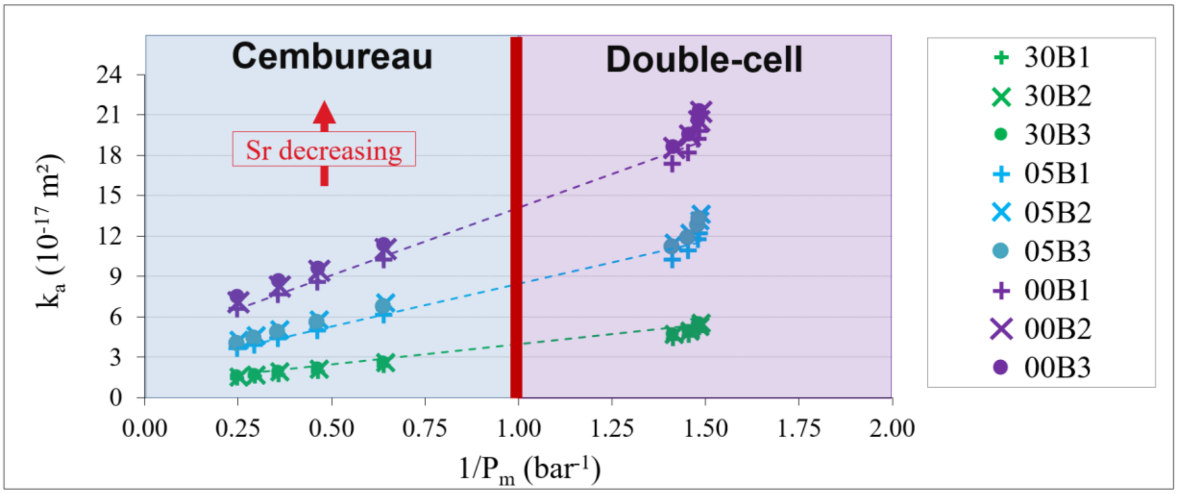


(b)

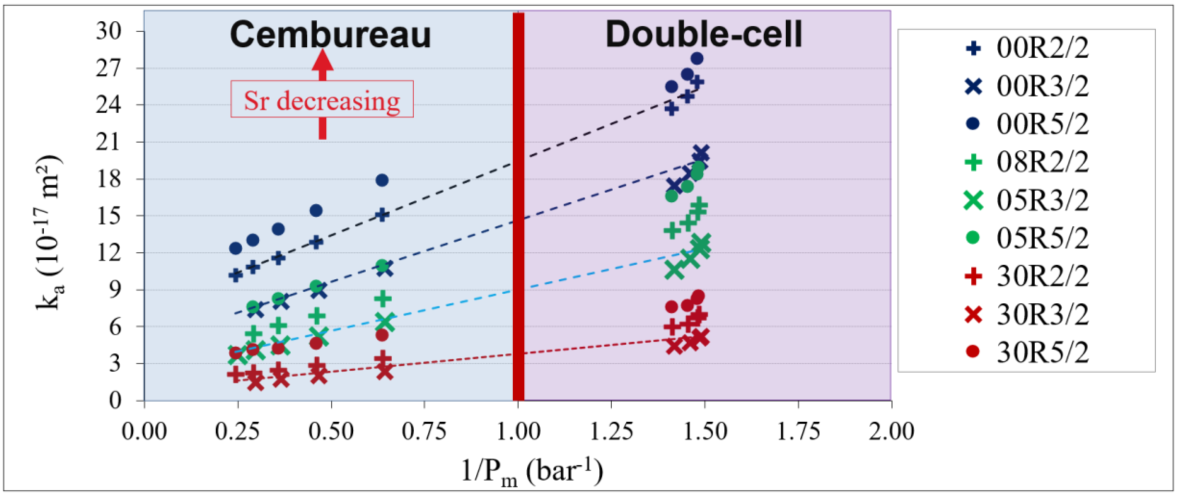


(c)

*Figure 7**:** Apparent permeability and Klinkenberg lines for plain samples of two different batches (a and b) and for samples with embedded steel bars (c)*

As illustrated in Figure 7-a, if Klinkenberg lines are plotted from the apparent permeability obtained under vacuum, high slopes are obtained, and a loss of linearity is observed: the non-laminar contribution is greater in a vacuum, and molecular flow increases as the vacuum becomes harder. This mechanism leads to obtain higher slopes under vacuum than under pressure. As a result, linear extrapolation of the experimental points leads to negative intrinsic permeability. This representation of Klinkenberg theory does not allow intrinsic permeability to be estimated but seems indicative of the evolution in molecular flow with the vacuum. Moreover, it highlights the difference of flow nature between the two techniques.

Nevertheless, for each sample at any saturation degree, the apparent permeability under vacuum obtained with the double-cell technique and plotted versus the inverse of the mean pressure is located near the reference Klinkenberg line established from the Cembureau measurement. For low pressures, the points deviate from the line, which also reflects the limits of Klinkenberg's approach at these pressures.

Experimental results can also be analysed with regard to the relative permeability for the quantification of the permeability evolution with saturation degree. It is defined as:

$$k_{Sr,Rel} = \frac{k_{Sr}}{k_{Srf}} \qquad \text{(Eq. 26)}$$

where $k_{Sr,Rel}$ is the relative permeability as a function of the saturation degree, $k_{Sr}$ is the permeability at a given saturation degree and $k_{Srf}$ is the permeability at the lowest saturation degree reached during the drying. The $k_{Srf}$ considered in this study is obtained for Sr = 3% after drying at 80 °C to constant mass.

As it has been well described in the literature [2], [9], [19], [36], the concrete permeability increases when the saturation degree decreases: during drying, the flow paths are released from the free water and the air flow through concrete can increase. Moreover, drying can induce damage and micro-cracking that increases the percolating network. This expected result is effectively obtained for the two techniques. Figure 8 presents the relative apparent permeability for the two techniques used in this paper for $P_I$ = 2 bars (Cembureau) and $P_O$ = 250 mbars (double-cell) and the relative intrinsic permeability.

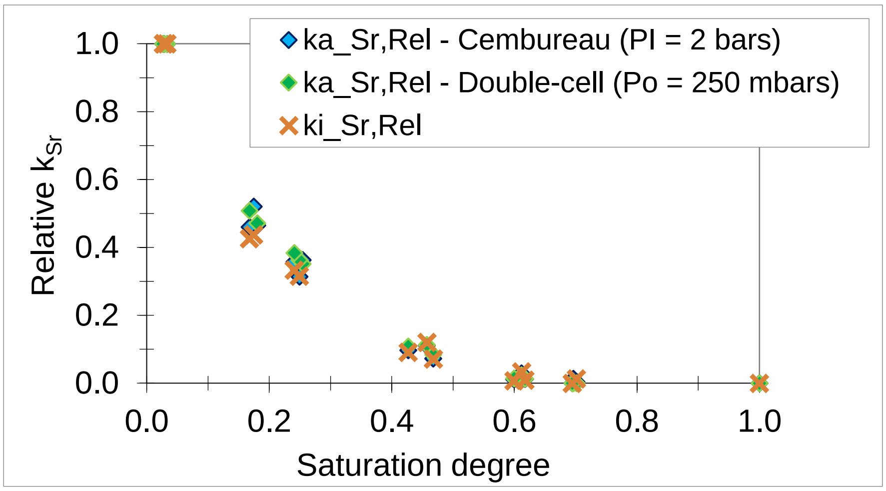


*Figure 8: Relative permeability according to saturation degree*

Whatever the type of permeability used (intrinsic permeability according to Klinkenberg, $k_i$, apparent permeability, $k_{a2bars}$, with the Cembureau technique, apparent permeability, $k_{a250mbars}$, with the double-cell technique), the evolutions of the relative permeability with the saturation degree were similar. This means that, without any other numerical processing, the apparent permeability obtained with the double-cell technique (or with the Cembureau technique) can be used to characterize the relative permeability.

### 5.1.2 Validation of the theoretical approach for permeability

The objective is to determine $k_{a2bars}$ and $k_i$ from any single apparent permeability given by the double-cell technique. Here is an example of the calculation protocol when the input data is apparent permeability obtained with the double cell for $P_O$ = 250 mbars: $k_{a250mbars}$.

- For $P_O$ = 250 mbars, $C_P$ = 0.63 in Table 1. Then (Eq. 13) gives the value of $k_{a2bars}$.
- With this value of $k_{a2bars}$ and with (Eq. 13), we calculate: $k_{a3bars}$ ($C_P$ = 1.17 in Table 1), $k_{a4bars}$ ($C_P$ = 1.30 in Table 1), $k_{a5bars}$ ($C_P$ = 1.41 in Table 1)

Figure 9 presents the results of $k_{a2bars}$ and $k_i$ predictions when the input data are $k_{a250mbars}$ or $k_{a150mbars}$ or $k_{a0.5mbar}$.

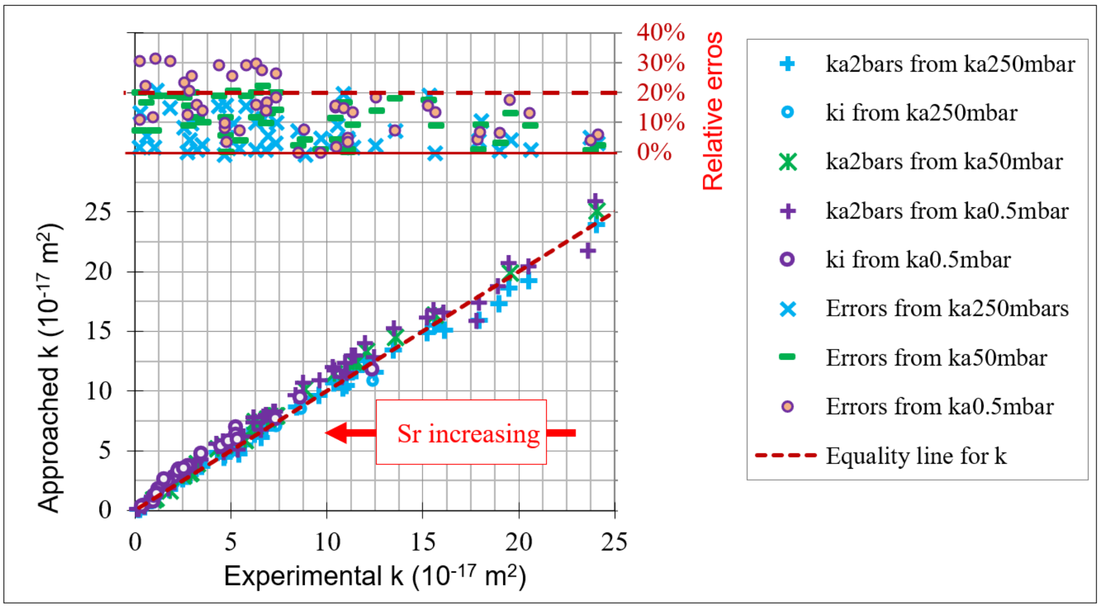


*Figure 9. Comparison of experimental and approached permeability*

The relative error between the permeability approximated with the proposed method and the experimental value $k_{a2bars}$ is also presented in Figure 9:

- The lowest vacuum pressure leads to the greatest relative error: this is in accordance with the assumption on flow regime. If the vacuum pressure is reduced, the flow rate no longer increases (between $P_O$ = 50 mbar and $P_O$ = 0.5 mbar the permeability increases by only 3%) whereas the molecular flow becomes more and more important, leading to the limits of use of Klinkenberg's theory. Then, for $k_{a2bars}$ and $k_i$ prediction with the double-cell technique, measurement should be performed with $P_O$ equal to or greater than 50 mbars.
- Using permeability for $P_O$ equal to or greater than 50 mbars, the relative error is always lower than 20%. Its mean value is about 7% and 12% when the calculations are done with $k_{a250bars}$ and $k_{a50mbar}$, respectively, which is considered as acceptable in this paper because of the usual deviation obtained on permeability measurement, which can reach 20% on 3 samples of a given batch.

The values of the coefficients $C_P$ (Table 1) are thus validated on the concrete studied in this work for various saturation degrees. The proposed approach makes it possible to estimate the apparent and intrinsic permeability from one value of apparent permeability.

The theoretical approach is also validated on experimental literature values. The objective is to determine apparent permeability at any pressure and the intrinsic permeability $k_i$ from a single apparent permeability $k_{a2bars}$ using (Eq. 13) and the value of $C_P$ presented in Table 1, for concrete of other experiments drawn from the literature. The apparent permeability must be calculated separately for inlet pressures, $P_I$, equal to 3, 4 and 5 bars:

- Calculation of $k_{a3bars}$: $P_m$ = 2.18 and $C_P$ = 1.18 in Table 1,
- Calculation of $k_{a4bars}$: $P_m$ = 2.81 and $C_P$ = 1.31 in Table 1,
- Calculation of $k_{a5bars}$: $P_m$ = 3.46 and $C_P$ = 1.42 in Table 1,
- Plot of calculated apparent permeability versus $1/P_m$ to deduce $k_i$.

Figure 10 presents the materials and the results ($k_{a5bars}$ and $k_i$; the predicted $k_{a4bars}$ and $k_{a3bars}$ show the same concordance) of this calculation protocol.

Porosity values are given for information. Porosity shows the porous extent of the concrete used to validate the value of $C_P$ proposed in this work. The relative errors between the experimental values and the values evaluated by this method is less than 20%, which is acceptable according accuracy on experimental measurement [16].

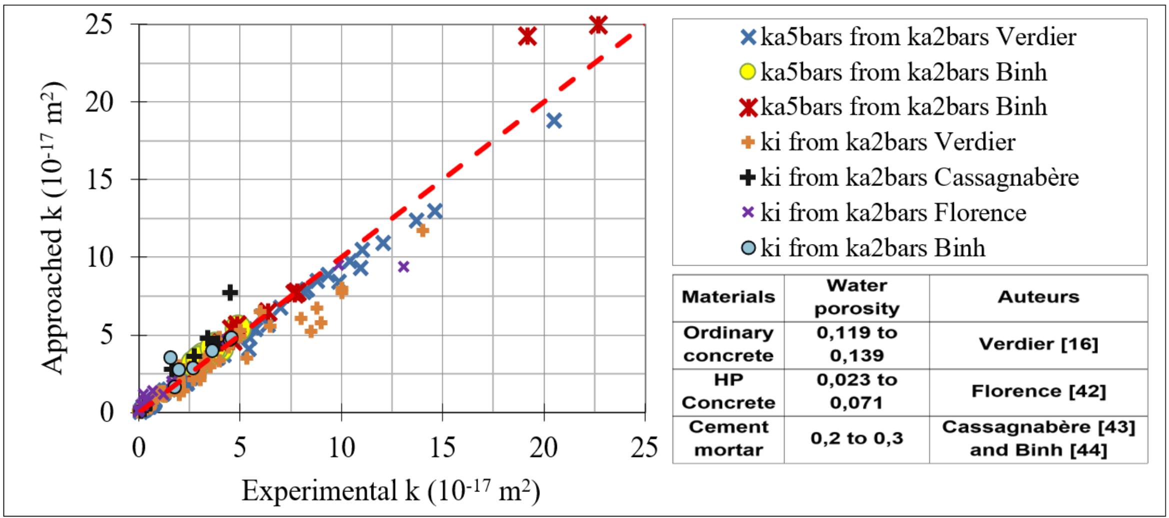


| Materials | Water porosity | Auteurs |
|---|---|---|
| Ordinary concrete | 0,119 to 0,139 | Verdier [16] |
| HP Concrete | 0,023 to 0,071 | Florence [42] |
| Cement mortar | 0,2 to 0,3 | Cassagnabère [43] and Binh [44] |

[16] [37] [38] [39]

*Figure 10: Validation of $C_P$ values on literature data*

## 5.2 Porosity accessible to gas

### 5.2.1 Experimental results of the Time to Reach Steady State (TRSS)

The porosity can be evaluated from the Time to Reach Steady State (TRSS) with (Eq. 25). First, Figure 11-a compares the Time to Reach Steady State (TRSS) obtained with the two techniques studied in this paper (under pressure in abscissa and under vacuum in ordinate). The TRSS obtained with the two techniques are almost equal but the TRSS with Cembureau are always slightly higher than those obtained with the double-cell technique. The apparent permeability under vacuum (obtained with double-cell) is always higher than the permeability obtained under pressure (with Cembureau). As the porous network is the same, the time necessary for the gas particles to cross the network (TRSS) is shorter under vacuum. As for permeability, it is interesting to analyse the relative TRSS. In this work, the relative TRSS was defined as the relative permeability (ratio of the TRSS obtained for a given saturation degree to the TRSS obtained for sample with a saturation degree of 3%).

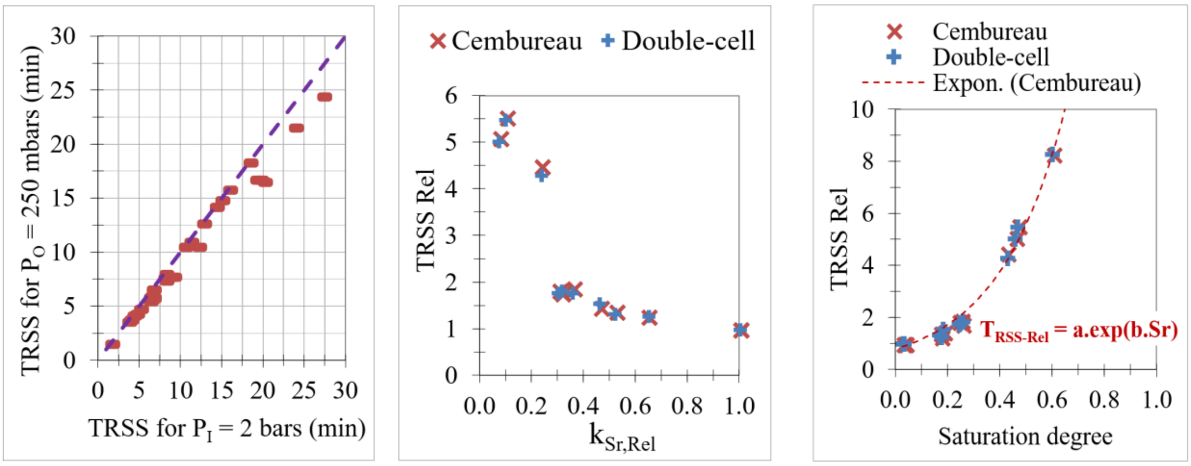


(a) (b) (c)

*Figure 11: TRSS with double-cell and Cembureau techniques (a), permeability (b) and TRSS as function of saturation degree (c)*

Figure 11-b presents the evolution of relative TRSS as a function of the relative permeability. When the relative permeability increases, the TRSS decreases. Considering that the TRSS is a function of the percolation path (tortuosity, constrictivity**,** rugosity, pore distribution), the impact of the pore tortuosity appears to be reduced for the highest permeability. The steady state is reached quickly when the air molecules encounter few obstacles in the porous network. Figure 11-c presents the evolution of TRSS as a function of the saturation degree and confirms this analysis. When the saturation degree decreases, the flow paths become progressively free of water and so air molecules encounter fewer obstacles and the steady state is reached faster, and permeability increases.

An empirical model of relative TRSS can be proposed:

$$T_{RSS_{Rel}} = a.\exp(b.Sr) \qquad \text{(Eq. 27)}$$

where $a$ and $b$ are two parameters established experimentally for each type of material. For the two batches of concrete tested in this paper $a$ and $b$ values are 0.78 and 3.92 for the plain samples (Figure 11-c). It is important to note that the same values of $a$ and $b$ are obtained with the Cembureau technique as with the double-cell technique. The double-cell technique can characterize the evolution of the transport properties of concrete according to saturation degree.

### 5.2.2 Validation of the theoretical approach for porosity

Figure 12 presents the porosity accessible to gas evaluated from TRSS (Eq. 25) for plain samples with the two techniques (Cembureau and double-cell) and the theoretical porosity evaluated from the total porosity accessible to water ((Eq. 1) and (Eq. 2)). Apparent permeability $k_{a2bars}$ is also plotted in blue on a secondary axis, for comparative analysis in Figure 12. In the case of very low permeability, the measurement of air flow may be not possible (case of sample 60B1 with the double-cell technique in Figure 12). The air flow is then equal to zero and there is no evaluation of TRSS, so the porosity deduced from the new approach is equal to zero, which is not necessarily true.

When the measurement of air flow is possible with the two techniques, the porosity accessible to gas obtained with both techniques is very similar (Figure 12): the absolute dispersion between the two techniques is 0.4% ± 0.2%. This is within the range of the accuracy on the measurement of porosity accessible to gas with the TRSS as presented in Figure 12. Concerning the comparison with the measurement under water, the results show similar trends according to the sample.

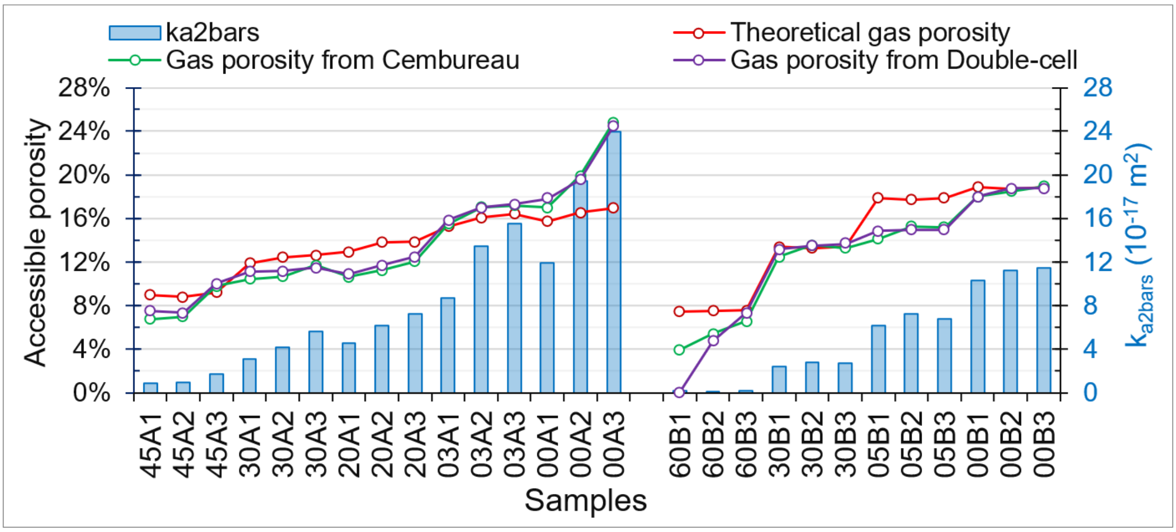


*Figure 12: Accessible porosity from different models on plain samples for two batches A and B (theoretical porosity is evaluated from total porosity accessible to water (Eq. 1))*

For most of the samples, the porosity deduced from measurement under water is higher than the porosity measured by gas transfer (Figure 12). This can be explained by the fact that the water porosity is the total accessible porosity whereas the porosity accessible to gas is the porosity that contributes to percolation paths during permeability test.

During the usual measurement, water can partly fill some dead arms. For the porosity calculated from TRSS through a permeability test, the porosity evaluated has to contribute to the gas transfer paths. As a result, theoretical porosity deduced from water porosity evaluates both open connected porosity and open non-connected porosity, while the porosity deduced from the TRSS is very little affected by the open non-connected porosity. Thus, the porosity calculated from the TRSS seems to be more representative of open-connected porosity. This approach should be validated on other materials such as porous ceramics.

In some cases, the porosity deduced from measurement under water is smaller than the porosity measured by gas transfer. This is mainly the case for saturation degrees lower than 3% for the first batch (A) for samples presenting the largest permeability (Figure 12). It is particularly marked for two samples. The high permeability measured in these samples can be explained by the creation of preferential paths of transfer during the last drying periods at 105 °C [40], [41]. Such paths can have large impacts on the transfer, and thus on the porosity deduced from transfer, while the consequences for the apparent porosity volume are very slight.

A comparison between the data of samples of the two batches 00A and 00B can complete this analysis. It introduces the problem of the analysis of the permeability from water porosity. The water porosity of samples 00B (around 19%) is higher than the water porosity of samples 00B (around 16%), but the permeability of samples 00B (12 x $10^{-17}$ $m^2$) is lower than the permeability of samples 00A (around 22 x $10^{-17}$ $m^2$). This points out that the water porosity cannot be effectively representative of gas percolation paths and so of gas permeability.

This result is more appreciable when we consider the results obtained on reinforced concrete samples (Figure 13). Previous analyses have shown that only significant preferential percolation paths can explain the differences of permeability of these samples [9], [19]. In Figure 13, samples 30B, 05B and 00B are plain samples while all the other results are obtained on reinforced samples (Figure 1). It appears clearly that the theoretical porosity accessible to gas (deducted from the water porosity) cannot explain the changes in permeability of these reinforced samples. The theoretical porosity indicates that the reinforced samples and the plain samples have approximately the same porosity while the permeability of reinforced samples is sometimes twice that of plain samples.

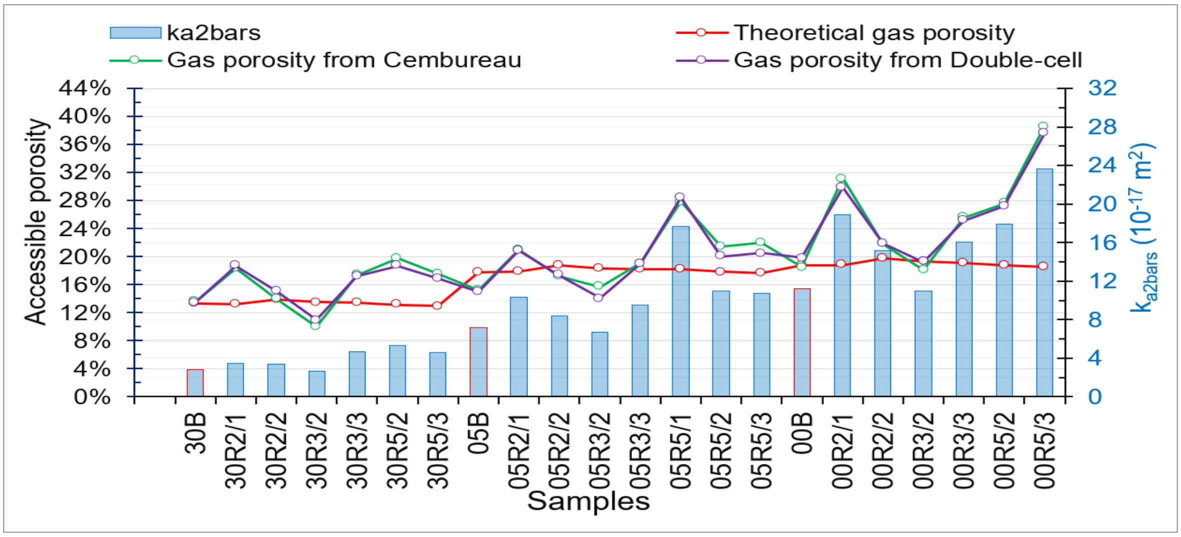


*Figure 13: Accessible porosity calculated from water porosity and from TRSS*

Only the porosities calculated from the TRSS as proposed in this study are sensitive to the defect created by steel bar in these samples and enable the samples to be distinguished from one another. The porosity calculated from apparent permeability and the TRSS thus appears to be more representative of the gas percolation paths.

### 5.2.3 Discussion

There are some theoretical limits on the proposed approach for porosity calculation. In presence of very high permeability or damaged samples, the TRSS should be much reduced and so its experimental evaluation could be tainted with error. The lowest value of TRSS in this paper was around 250 seconds with a maximum relative error equal to 3%, corresponding to an absolute error of 7.5 seconds. For samples with TRSS around 30 seconds [31], and with an absolute error of 7 seconds, the relative error becomes about 23%. This may lead to a considerable error in the porosity calculation. Another limit of the proposed approach is that the porosity calculated from TRSS is the porosity accessible to gas at the moment of the permeability test for a given saturation degree.

Relative permeability can be assessed as a function of saturation degree [42] (Figure 8). In this paper, it has been showed that the relative TRSS can also be evaluated as a function of saturation degree (Figure 11-c). Combining these two empirical laws and the theoretical relation between permeability, porosity and TRSS (Eq. 24) can lead to consistent prediction of the porosity accessible to gas for a concrete. For the purpose of more reliable modelling of transport into partially saturated concrete, there are two principal input data [29]: the permeability and the porosity. When the given porosity is not representative of the path accessible to gas, a third experimental data can be used to deduce the porosity accessible to gas transfer (Eq. 24): the time to reach steady state (TRSS).

# 6 Conclusion

The main objectives of this study have been to compare different techniques to determine the apparent and intrinsic permeability and the porosity of concrete. Three specifics points were studied: establishment of an experimental database on concrete air permeability and time to reach steady state, analysis of transfer properties through permeability calculations, and assessment of the porosity accessible to gas.

For the first time, air flow through concrete has been measured in vacuum with a double-cell device and under pressure with the Cembureau technique in the steady state for identical samples. The apparent permeability in low vacuum at steady state was calculated from the Hagen Poiseuille equation and compared to the under-pressure technique for the same samples. This apparent permeability obtained in vacuum from the double-cell was clearly efficient for the determination of the relative permeability.

The second goal of this paper has been the analysis of transfer properties through permeability calculation. The characteristic apparent permeability, $k_{a2bars}$, was calculated from one apparent permeability given by the double-cell technique. This characteristic permeability was compared to the apparent permeability measured directly with the Cembureau technique. An original relation between apparent permeability at different pressures was proposed and validated, and the results showed good agreement between prediction and experimental measurements.

Concerning the Time to Reach Steady State (TRSS), this study shows that this parameter can be used to analyse the percolation paths regardless of the techniques used (double-cell or Cembureau). An empirical relation was established for the relative TRSS as a function of saturation degree. The porosity accessible to gas was calculated from a new relation between the TRSS and the apparent permeability (or volumetric air flow). The results obtained from the Cembureau technique and those obtained with the double-cell technique were in good concordance. Moreover, these results obtained show that this porosity should be more convincing than the water porosity for the evaluation of the percolation paths accessible to gas.

## 7 Acknowledgment

The authors acknowledge the financial support provided by the project “Non-destructive evaluation of containment of nuclear power plants” (ENDE) financed by the Programme Investissement d’Avenir (PIA – Centre National de la Recherche Scientifique, délégation Provence et Corse, France).

## 8 Conflict of Interest statement

**Conflict of Interest**: The authors declare that they have no conflict of interest.

## 9 References

[1] H. Hilsdorf and J. Kropp, *Performance Criteria for Concrete Durability*. CRC Press, 2004.

[2] A. Abbas, M. Carcasses, and J.-P. Ollivier, “Gas permeability of concrete in relation to its degree of saturation,” *Mater. Struct.*, vol. 32, no. 1, pp. 3–8, 1999.

[3] L. Basheer, J. Kropp, and D. J. Cleland, “Assessment of the durability of concrete from its permeation properties : a review,” *Constr. Build. Mater.*, vol. 15, no. 2–3, pp. 93–103, Mar. 2001.

[4] J.-P. Ollivier, J.-M. Torrenti, and M. Carcasses, *Propriétés physiques du béton et de ses constituants*. Hermes, Lavoisier, 2012.

[5] F. Ghasemzadeh, R. Rashetnia, D. Smyl, and M. Pour-Ghaz, “A comparison of methods to evaluate mass transport in damaged mortar,” *Cem. Concr. Compos.*, vol. 70, pp. 119–129, Jul. 2016.

[6] AFPC-AFREM, *Compte-rendu des journées techniques AFPC/AFREM. Durabilité des bétons, “Méthodes recommandées pour la mesure des grandeurs associées à la durabilité”, 11 and 12 december 1997, LMDC Toulouse / Réf. ATILH n°37864*. 1997.

[7] Norme XP P18-463, *Norme XP P18-463 - Essai pour béton durci - Essai de perméabilité à l’air*. 1999.

[8] V. Picandet, “Influence d’un endommagement mécanique sur la perméabilité et sur la diffusivité hydrique des bétons,” Ph.D. Thesis, Ecole Centrale de Nantes, 2001.

[9] H. E. A. Sogbossi, “Etude de l’évolution de la perméabilité du béton en fonction de son endommagement : transposition des résultats de laboratoire à la prédiction des débits de fuite sur site,” Ph.D. Thesis, Université de Toulouse, Université Toulouse III - Paul Sabatier, 2017.

[10] C. Villani, R. Loser, M. J. West, C. Di Bella, P. Lura, and W. J. Weiss, “An inter lab comparison of gas transport testing procedures : Oxygen permeability and oxygen diffusivity,” *Cem. Concr. Compos.*, vol. 53, pp. 357–366, Oct. 2014.

[11] P. C. Carman, *Flow of Gases Through Porous Media*. Academic Press, 1956.

[12] D. Hoffman, B. Singh, and J. H. Thomas III, *Handbook of vacuum science and technology*. Academic Press, 1997.

[13] L. J. Klinkenberg, “The permeability of porous media to liquids and gases,” *Drilling and production practice, American Petroleum Institute*, 01-Jan-1941.

[14] A. S. Ziarani and R. Aguilera, “Knudsen’s permeability correction for tight porous media,” *Transp. Porous Media*, vol. 91, no. 1, pp. 239–260, Jan. 2012.

[15] D. Perraton, P.- Aitcin, and A. Carles-Gibergues, “Mesure de la permeabilité aux gaz des bétons : permeabilité apparente et permeabilité intrinsèque. Partie I - Validation des concepts de Carman et de Klinkenberg dans le cas d’un BHP,” *Bull. Lab. Ponts Chaussées*, no. 221, May 1999.

[16] J. Verdier, “Contribution à la caractérisation de l’évolution du taux de fuite des enceintes de confinement du parc nucléaire,” Ph.D. Thesis, Université de Toulouse, Université Toulouse III-Paul Sabatier, 2001.

[17] Norme NF P18-459, *Norme NF P18-459 - Béton - Essai pour béton durci - Essai de porosité et de masse volumique*. 2010.

[18] V. Baroghel-Bouny *et al.*, “Méthodes d’essai N°58 : Caractéristiques microstructurales et propriétés relatives à la durabilité des bétons : Méthodes de mesure et d’essai de laboratoire,” *Tech. Méthodes Lab. Ponts Chaussées-LCPC Cerca Con Google*, 2002.

[19] H. Sogbossi, J. Verdier, and S. Multon, “Impact of reinforcement-concrete interfaces and cracking on gas transfer in concrete,” *Constr. Build. Mater.*, vol. 157, pp. 521–533, Dec. 2017.

[20] V. Garnier, “Evaluation non destructive des enceintes de confinement des centrales nucléaires - Compte rendu de la Réunion plénière N°6,” ISFTTAR, Nantes, Jan. 2017.

[21] R. J. Torrent, “A two-chamber vacuum cell for measuring the coefficient of permeability to air of the concrete cover on site,” *Mater. Struct.*, vol. 25, no. 6, pp. 358–365, 1992.

[22] J.-P. Ollivier and J.-M. Torrenti, “La structure poreuse des bétons et les propriétés de transfert,” *Durabilité Bétons*, vol. 1, 2008.

[23] A. Lobet, *Influence des paramètres de composition des matériaux cimentaires sur les propriétés de transfert*. Ph.D. Thesis, Toulouse, INSA, 2003.

[24] J. J. Kollek, “The determination of the permeability of concrete to oxygen by the Cembureau method-a recommendation,” *Mater. Struct.*, vol. 22, no. 3, pp. 225–230, 1989.

[25] C. Antón, M. A. Climent, G. de Vera, I. Sánchez, and C. Andrade, “An improved procedure for obtaining and maintaining well characterized partial water saturation states on concrete samples to be used for mass transport tests,” *Mater. Struct.*, vol. 46, no. 8, pp. 1389–1400, Nov. 2012.

[26] RILEM TC 116-PCD, “Permeability of concrete as a criterion of its durability, final report,” *Mater. Struct.*, vol. 32, no. 217, pp. 163–173, Apr. 1999.

[27] M. Carcassès, A. Abbas, J.-P. Ollivier, and J. Verdier, “An optimised preconditioning procedure for gas permeability measurement,” *Mater. Struct.*, vol. 35, no. 1, pp. 22–27, 2001.

[28] S. Dushman and Research Staff of General Electric Research Laboratory, “Scientific foundations of vacuum technique,” *Am. J. Phys.*, vol. 30, no. 8, pp. 612–612, 1962.

[29] J. Verdier, M. Carcassès, and J. P. Ollivier, “Modelling of a gas flow measurement : Application to nuclear containment vessels,” *Cem. Concr. Res.*, vol. 32, no. 8, pp. 1331–1340, Aug. 2002.

[30] Y.-S. Wu, K. Pruess, and P. Persoff, “Gas Flow in Porous Media With Klinkenberg Effects,” *Transp. Porous Media*, vol. 32, no. 1, pp. 117–137, Jul. 1998.

[31] D. Gardner, “Experimental and numerical studies of the permeability of concrete,” Ph.D. Thesis, Cardiff University, 2005.

[32] G. E. Karniadakis, A. Beskok, and N. Aluru, *Microflows and Nanoflows: Fundamentals and Simulation*. Springer Science & Business Media, 2005.

[33] S. Roy, R. R. F. Chuang, B. A. Cruden, and M. Meyyappan, “Modeling gas flow through microchannels and nanopores,” *J. Appl. Phys.*, vol. 93, no. 8, pp. 4870–4879, Mar. 2003.

[34] J. F. O'Hanlon, *A user's guide to vacuum technology*, 3rd edition. John Wiley & Sons, 2005.
[35] N. P. Pham, A. Toumi, and A. Turatsinze, "Effect of Styrene-Butadiene Copolymer Coating on Properties of Rubberized Cement-Based Composites," in *Strain-Hardening Cement-Based Composites*, vol. 15, V. Mechtcherine, V. Slowik, and P. Kabele, Eds. Dordrecht: Springer Netherlands, 2018, pp. 342–350.
[36] J. Verdier and M. Carcassès, "Equivalent gas permeability of concrete samples subjected to drying," *Mag. Concr. Res.*, vol. 56, no. 4, pp. 223–230, May 2004.
[37] F. A. Florence, J. Rushing, K. E. Newsham, and T. A. Blasingame, "Improved Permeability Prediction Relations for Low Permeability Sands," 2007.
[38] F. Cassagnabère, "Produits préfabriqués en béton filé : vers l'amélioration des performances du matériau pour mieux gérer le procédé de production," PhD Thesis, Université de Toulouse, Université Toulouse III-Paul Sabatier, 2007.
[39] M. Binh, "Etude de la perméabilité des mortiers de ciment soumis à l'alcali réaction," Rapport de stage de recherche, Université de Toulouse, Université Toulouse III-Paul Sabatier, 2007.
[40] P. Van den Heede, E. Gruyaert, and N. De Belie, "Transport properties of high-volume fly ash concrete: Capillary water sorption, water sorption under vacuum and gas permeability," *Cem. Concr. Compos.*, vol. 32, no. 10, pp. 749–756, Nov. 2010.
[41] J. Castro, D. Bentz, and J. Weiss, "Effect of sample conditioning on the water absorption of concrete," *Cem. Concr. Compos.*, vol. 33, no. 8, pp. 805–813, 2011.
[42] M. T. Van Genuchten, "A closed-form equation for predicting the hydraulic conductivity of unsaturated soils," *Soil Sci. Soc. Am. J.*, vol. 44, no. 5, pp. 892–898, 1980.